iScience

CellPress
OPEN ACCESS

Article

Cholinergic Modulation of the Default Mode Like Network in Rats

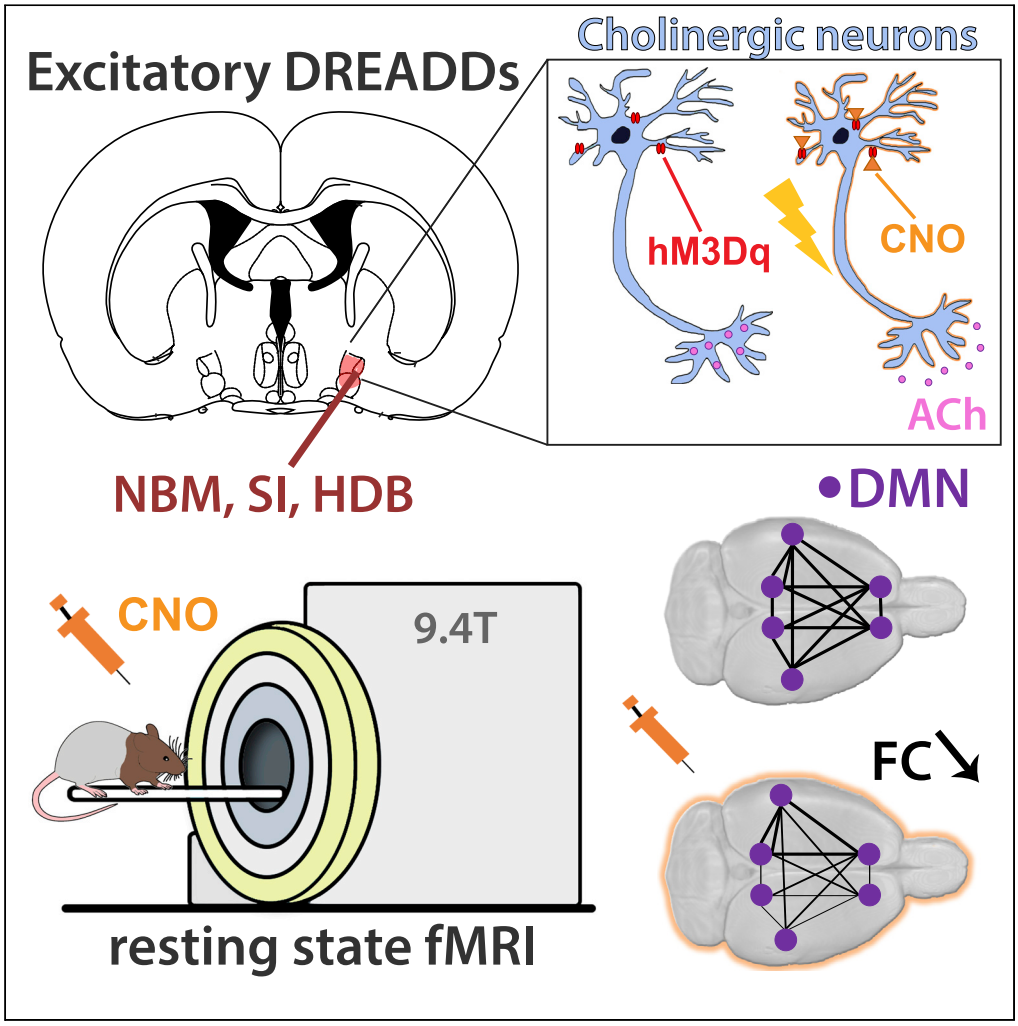

Lore M. Peeters, Monica van den Berg, Rukun Hinz, Gaurav Majumdar, Isabel Pintelon, Georgios A. Keliris

georgios.keliris@uantwerpen.be

HIGHLIGHTS

We expressed DREADDs in the cholinergic neurons of the right basal forebrain (BFB)

We provide a tool to selectively modulate the default mode like network (DMLN)

Cholinergic stimulation decreases functional connectivity (FC) in the DMLN

Stimulation of right BFB induces lateralized effects on FC in DMLN and TPN

Peeters et al., iScience *23*, 101455
September 25, 2020
https://doi.org/10.1016/j.isci.2020.101455

iScience

CellPress
OPEN ACCESS

Article

Cholinergic Modulation of the Default Mode Like Network in Rats

Lore M. Peeters,[1,3] Monica van den Berg,[1,3] Rukun Hinz,[1] Gaurav Majumdar,[1] Isabel Pintelon,[2] and Georgios A. Keliris[1,4,*]

SUMMARY

The discovery of the default mode network (DMN), a large-scale brain network that is suppressed during attention-demanding tasks, had major impact in neuroscience. This network exhibits an antagonistic relationship with attention-related networks. A better understanding of the processes underlying modulation of DMN is imperative, as this network is compromised in several neurological diseases. Cholinergic neuromodulation is one of the major regulatory networks for attention, and studies suggest a role in regulation of the DMN. In this study, we unilaterally activated the right basal forebrain cholinergic neurons and observed decreased right intra-hemispheric and interhemispheric FC in the default mode like network (DMLN). Our findings provide critical insights into the interplay between cholinergic neuromodulation and DMLN, demonstrate that differential effects can be exerted between the two hemispheres by unilateral stimulation, and open windows for further studies involving directed modulations of DMN in treatments for diseases demonstrating compromised DMN activity.

INTRODUCTION

An important finding in neuroscience during the last couple of decades was the discovery of the default mode network (DMN), which is a large-scale network of brain areas that are co-activated during passive mental processes and suppressed during externally oriented attention-demanding cognitive tasks. This was initially observed by Shulman et al. (1997) in a meta-analysis of nine positron emission tomography (PET) studies. In that study, the authors showed that several brain areas, including the medial prefrontal cortex, posterior cingulate cortex, and lateral parietal and temporal cortices, consistently increased their metabolic activity during states of rest or quiet wakefulness (Shulman et al., 1997). Functional imaging studies, which followed, reported that the low-frequency activity fluctuations of these areas were highly temporally correlated, forming a set of intrinsically functionally connected brain areas currently known as the default mode network (DMN) (Greicius et al., 2003; Raichle et al., 2001; Raichle and Snyder, 2007). The DMN has been associated with spontaneous internally directed cognitive processes such as mind wandering, self-oriented processes, and introspection (Andrews-Hanna et al., 2010; Buckner and Carroll, 2007). Disruption of DMN functioning has been linked to several neurological disorders, including attention deficit hyperactivity disorder (Tian et al., 2006), mood disorders (Greicius et al., 2007), epilepsy (Laufs et al., 2007), Alzheimer's disease (Greicius et al., 2004) and others (Broyd et al., 2009). Upon the discovery of the DMN in humans, a default mode like network (DMLN) has been observed in several other mammalian species, such as the macaque monkey (Vincent et al., 2007), rat (Lu et al., 2012), and mouse (Stafford et al., 2014). In rodents, DMLN consists of the following brain regions: orbital cortex, prelimbic cortex, cingulate cortex, auditory/temporal association cortex, posterior parietal cortex, retrosplenial cortex, and hippocampus (Lu et al., 2012; Stafford et al., 2014). Multiple studies observed shared features of the DMN in humans and the DMLN in rodents, i.e., its anatomical homology (Lu et al., 2012), its link with brain disorders (Sforazzini et al., 2016; Anckaerts et al., 2019; Shah et al., 2016), its decreased activity during tasks in comparison with rest (Hinz et al., 2019; Rohleder et al., 2016) and its anti-correlation with task-positive networks (TPNs) (Schwarz et al., 2013; Belloy et al., 2018).

The DMN has also been described as a "task-negative network," which exhibits anti-correlations with "task-positive networks" (Greicius et al., 2003; Fox et al., 2005; Belloy et al., 2018). The antagonistic interaction

[1]Bio-Imaging Lab, University of Antwerp, Campus Drie Eiken – Universiteitsplein 1, 2610 Wilrijk, Belgium

[2]Laboratory of Cell Biology and Histology, University of Antwerp, Universiteitsplein 1, 2610 Wilrijk, Belgium

[3]These authors contributed equally

[4]Lead Contact

*Correspondence: georgios.keliris@uantwerpen.be

https://doi.org/10.1016/j.isci.2020.101455

between the DMN and top-down attentional processes has been observed repeatedly in humans (Buckner and Dinicola, 2019); however, the underlying mechanisms remain poorly understood. A number of previous studies have shown that the extent and the magnitude of the task-induced decreases in BOLD responses within the DMN vary with the difficulty of the cognitive tasks and that task performance is positively correlated with the strength of the DMN suppression (Rajan et al., 2019; Ossandon et al., 2011; Wen et al., 2013; Mayer et al., 2010; Singh and Fawcett, 2008). Another important feature of the DMN, demonstrated by several human studies, is decreased functional connectivity (FC) within the network during the performance of cognitive tasks (Gao et al., 2013; Fransson, 2006). Interestingly, a recent study in humans demonstrated that the presentation of random flashing checkerboard visual stimuli can induce negative BOLD responses in DMN brain regions (Razlighi, 2018). Similarly, our group evaluated the BOLD responses in the DMLN regions upon the presentation of continuous flickering visual stimuli in sedated rats. We demonstrated that this visual stimulation paradigm could deactivate nodes of the DMLN and decrease the FC assimilating earlier studies in humans (Hinz et al., 2019).

Recent studies have demonstrated that the basal forebrain (BFB) is a key player in modulating oscillations in the prefrontal cortex during behaviors aligned with DMN activation and de-activation patterns, such as moving from the home cage to an experimental arena where exploration of the environment is enhanced, and suggested these findings are consistent with BFB exerting control of large-scale functional networks such as the DMN (Nair et al., 2018). This hypothesis is also consistent with evidence that cholinergic neurons originating from the BFB are strongly involved in attentional processes, specifically the projections from the diagonal band of Broca, substantia innominata, and the nucleus Basalis of Meynert (NBM) to the cortex (Ballinger et al., 2016; Bloem et al., 2014; Howe et al., 2017; Parikh et al., 2007). These projections induce acute increases of acetylcholine (ACh) in the medial prefrontal cortex, which mediate cue detection and are necessary for successful task performance (Howe et al., 2017; Gritton et al., 2016; Parikh et al., 2007). Moreover, ACh enhances visual processing by inducing cortical decorrelation and desynchronization in sensory cortices, which increases the signal to noise ratio (Chen et al., 2015; Nguyen et al., 2015; Pinto et al., 2013). Moreover, the BFB has been implicated in cortical network switching between brain states by exerting direct and/or indirect control to the prefrontal cortex (Espinosa et al., 2019b; Li et al., 2015).

This evidence suggested an involvement of the BFB cholinergic system in the up- and down-regulation of the DMN and its anti-correlation with task-based/attention-related networks. Thus, we hypothesized that specific stimulation of cholinergic neurons in the BFB can influence the functional connectivity (FC) in the DMLN of rats as measured with whole-brain measures of activity and connectivity such as resting-state (rs) fMRI, which can directly visualize the complete DMN and task-based networks. Furthermore, inspired by a recent study in rhesus macaques that demonstrated unilateral suppression of cortical fluctuations ipsilateral to pharmacological inactivations in the NBM (Turchi et al., 2018), we hypothesized that unilateral activations of cholinergic neurons in homologous areas in the rat could potentially lead to asymmetric changes to the DMLN that could be beneficial in the treatment of certain neurological syndromes that are thought to stem from hemispheric imbalances in attentional processes such as hemispatial neglect (Bartolomeo et al., 2012). To this end, we combined functional MRI with designer receptors exclusively activated by designer drugs (DREADDs) to selectively increase the neuronal firing in basal forebrain (BFB) cholinergic neurons and study their effects in whole brain networks with a particular focus on the DMLN. We found that unilateral cholinergic activation in the right BFB resulted in decreased FC in the DMLN and the effect showed significant laterality in specific connections in the DMLN and task-based networks. The results of this study directly demonstrate the effects of cholinergic neuromodulation in the DMLN in rats and open windows for further studies that could use directed modulations of DMLN in rehabilitation treatments for diseases demonstrating compromised DMN activity.

RESULTS

DREADDs Expression Co-Localizes with Cholinergic Neurons in the Right Basal Forebrain

Chemogenetic tools, such as DREADDs, allow control of the activity of selectively targeted neuronal populations (Alexander et al., 2009). In our study, excitatory DREADDs were used to increase the activity of cholinergic neurons in the right BFB. To ensure exclusive DREADDs expression in the cholinergic neurons of the right BFB, we used ChAT-Cre transgenic rats that selectively express Cre-recombinase in all choline acetyltransferase (ChAT)-expressing neurons, i.e., cholinergic neurons (Witten et al., 2011). The presence of Cre-recombinase allows the conversion of the inverted DNA constructs, so that gene transcription can take place. Viral vectors containing inverted DNA constructs encoding DREADDs were stereotactically injected

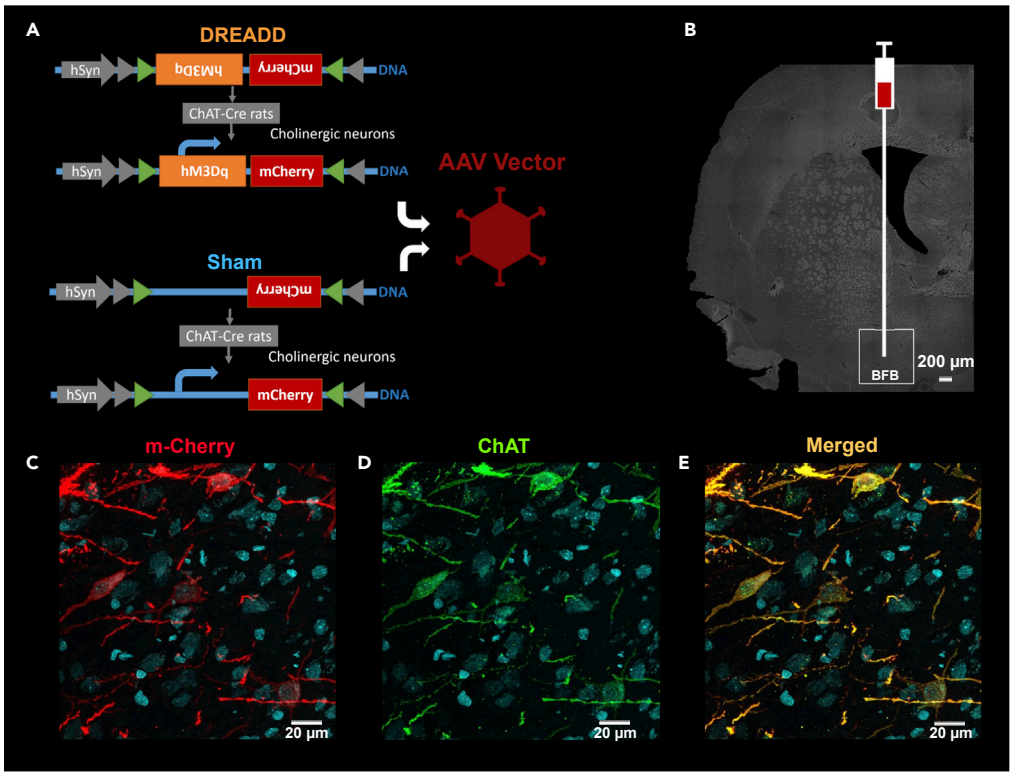

Figure 1. Expression of DREADDs in Basal Forebrain Cholinergic Neurons

(A) Graphical representation of the DREADDs construct and Adeno-associated viral vector. The viral construct contains an inverted DREADDs receptor (orange) and fluorescent m-Cherry label (Red). The Sham virus only contains the inverted fluorescent m-Cherry label (red). Cre recombinase (grey) is needed to convert the constructs to allow transcription. Transgenic ChAT-Cre rats were used, to allow expression of the DREADDs in the cholinergic neurons.

(B) Viral vectors containing the inverted DNA constructs encoding the DREADDs receptors were injected in the right basal forebrain (BFB) of the experimental group during a stereotactic surgery. Viral vectors with an empty DNA construct were injected in the right BFB of sham-treated animals. ChAT-cre transgenic rats were used in both groups.

(C–E) Immunohistochemistry was performed on eight animals to check the expression of the DREADDs. Representative maximum intensity projections are shown in which the expression of mCherry is represented in red and cell nuclei in blue. (C) mCherry expression is observed in the cell body and axons of the neurons. (D) ChAT, an enzyme present in cholinergic neurons, is presented in green. (E) Co-localization of mCherry and ChAT in yellow (red + green). Virtually all cholinergic neurons in the target region were transfected and no mCherry was observed in structures other than cholinergic neurons.

in the right BFB (Figure 1). Since cholinergic neurons in the anterior medial portion of the BFB have been shown to project to the medial and frontal cortex, and have been implicated to play a role in attention, these medial nuclei were targeted during the stereotactic surgery (Ballinger et al., 2016; Chaves-Coira et al., 2018). Immunohistochemical experiments were performed on eight animals to validate transfection of cholinergic neurons in the target region. The DREADDs were tagged with a fluorescent label (m-Cherry), which could be observed in the targeted medial nuclei of the basal forebrain, namely, the horizontal diagonal band of Broca, substantia innominata, and nucleus basalis of Meynert. Dual visualization of mCherry and ChAT, which is a specific marker for cholinergic neurons via immunohistochemistry, revealed co-localization of mCherry and ChAT in the right BFB (Figure 1). These results indicated successful cell-type-specific transfection of the cholinergic neurons in the selected regions in the right BFB.

DREADDs-Induced Neural Activity Modulation Exerts Its Effects on Functional Connectivity Acutely after Administration of Clozapine-N-oxide

First, the temporal profile of the DREADDs-induced FC changes within DMLN was evaluated. Regions of interest (ROIs) were drawn in brain regions of the DMLN in rats (Lu et al., 2012; Stafford et al., 2014), and their FC alterations were followed up over time after administration of clozapine-N-oxide (CNO). Significantly decreased FC in the right DMLN could be observed in the DREADDs-expressing rats starting at

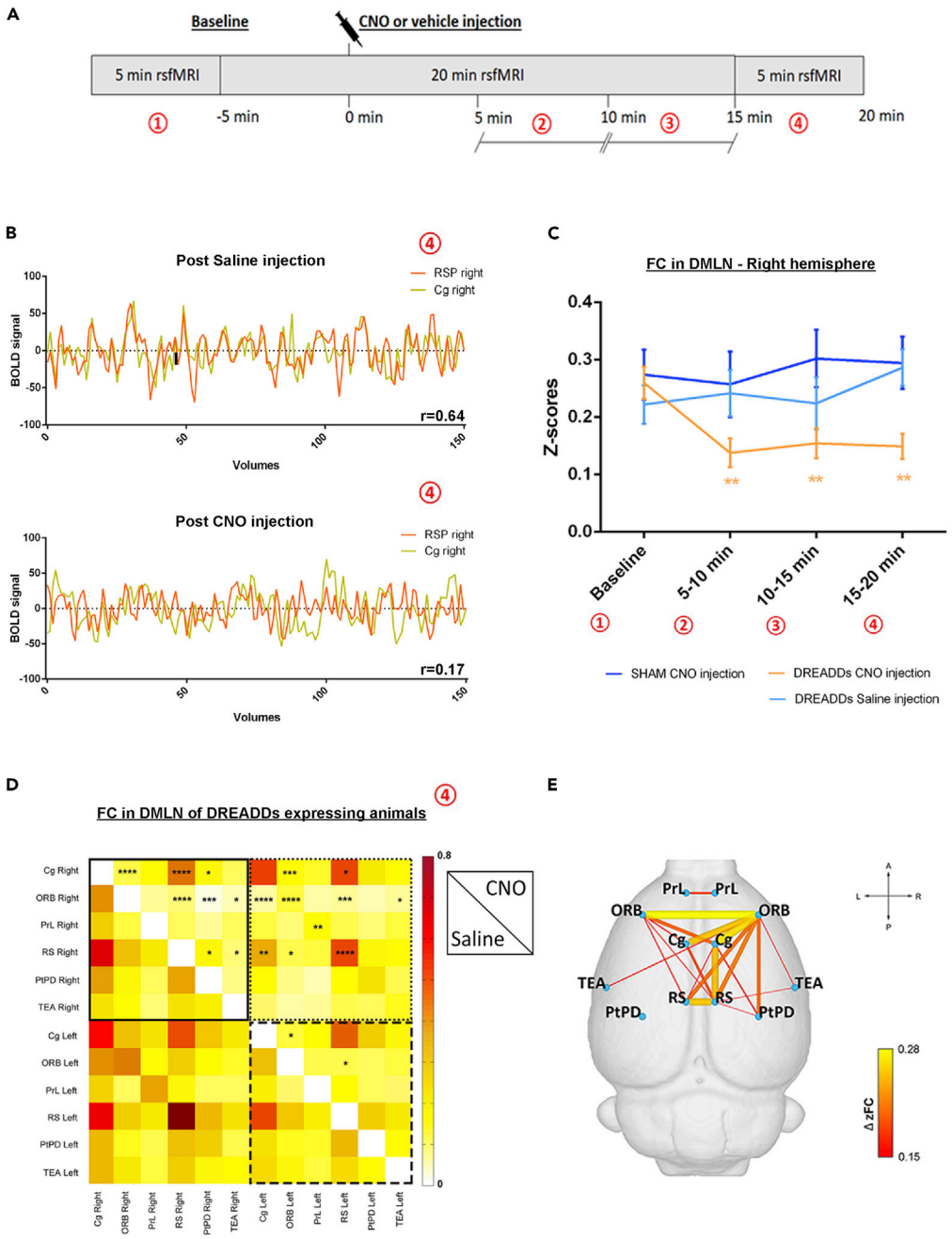

Figure 2. DREADDs-Induced Right Basal Forebrain (BFB) Stimulation Alters Functional Connectivity in the Default Mode like Network (DMLN)

(A) Timeline of the acquired rsfMRI scans during one scan session.

(B) Example of BOLD signal time courses from the right cingulate and right retrosplenial cortex in one DREADDs-expressing animal after saline (vehicle) and CNO injection. r-Values on the lower right corners show the Pearson correlation coefficient of the respective time courses.

(C) FC strength in units of Fischer-z transformed correlation (z-scores) ±SEM, in the right DMLN of the DREADDs-expressing group after CNO injection and saline injection as well as for the sham group after CNO injection. The time development of FC is shown at different time points: baseline, 5–10 min, 10–15 min, and 15–20 min after administration of CNO or saline (see A). The indicated significant differences were obtained by linear mixed model analysis with Student's t correction for multiple comparisons.

(D) Pairwise z-transformed FC matrix after saline injection (sub-diagonal) and after CNO injection (supra-diagonal) in the DREADDs-expressing group. The color bar represents z-scores. The stars indicate significant differences between the

Figure 2. *Continued*
saline injection and CNO injection (repeated measures two-way ANOVA with Sidak's correction for multiple comparisons).
(E) Illustration of the significantly decreased FC presented in (D) in a ball and stick diagram overlaid on a 3D anatomical template surface. The lines represent significant differences in the DREADDs group after CNO injection with the color scale representing the actual difference in FC between the two scans (saline versus CNO injection). Yellow indicates larger FC decrease after CNO injection. The z-scores of both groups were statistically compared using a paired Student's t test. *$p \leq 0.05$, **$p \leq 0.01$, ***$p \leq 0.001$, ****$p \leq 0.0001$. Abbreviations: Cg, cingulate cortex; ORB, orbitofrontal cortex; PrL, prelimbic cortex; RS, retrosplenial cortex; PtPD, parietal association cortex; TEA, temporal association cortex; FC, functional connectivity; DMLN, default mode like network; CNO, clozapine-N-oxide; DREADDs, designer receptors exclusively activated by designer drugs; min, minutes.

5–10 min post-CNO injection ($p = 0.002$, Figure 2C). Furthermore, this significantly decreased FC in the DMLN lasted at least until 20 min post-CNO injection (10–15 min: $p = 0.01$; 15–20 min: $p = 0.001$, Figure 2C). In contrast, CNO injection in the sham group ($p = 0.154$) or saline injection in the DREADDs-expressing animals (5–10 min: $p = 0.530$; 10–15 min: $p = 0.871$; 15–20 min: $p = 0.059$) did not elicit FC alterations.

Right Basal Forebrain Stimulation Induces Decreased Intra- and Inter-Hemispheric Functional Connectivity in Default Mode like Network

To better understand the effect of right BFB stimulation on bilateral DMLN FC, an ROI-based analysis was performed using DMLN ROIs across the hemispheres. First, the FC of DMLN regions after CNO injection and saline injection was compared in the DREADDs-expressing group. The CNO and saline injections were performed in the same group of animals during different scan sessions. These results demonstrated that CNO-induced stimulation of the right BFB cholinergic system significantly decreased the FC between various DMLN ROI pairs (Figure 2D). Additionally, comparing the average intra-hemispheric and inter-hemispheric FC of the DMLN between both groups revealed significantly decreased FC within the right hemisphere ($p = 0.002$) as well as between the hemispheres ($p = 0.007$). Next to the evaluation of the FC within the DMLN, a seed-based analysis was performed for seed regions in the right Cg and right RSP to assess alterations of the FC patterns across the brain. These analyses revealed that right BFB stimulation significantly decreased the FC for both seed regions (Figures 3A–3D). Furthermore, comparison of the DMLN FC between the sham group and the saline-injected DREADDs-expressing group showed no significant FC alterations (Figures S1A and S1B). Non-specific effects of CNO injection on the intra- and inter-hemispheric FC of the DMLN were evaluated by comparing the sham group with the DREADDs-expressing group after CNO injection. This analysis showed that the average FC in the right hemisphere and between both hemispheres significantly decreased only in the DREADDs-expressing rats (Figure S2). These results suggest that CNO injection did not induce non-specific effects on FC in the DMLN.

Right BFB Stimulation Induces Resting-State Neural Activity Decreases in DMLN

Next to the evaluation of FC alterations in the DMLN, the resting-state neural activity alterations in the DMLN were assessed by comparing the fractional amplitude of low-frequency fluctuations (fALFF [Zou et al., 2008]) values upon CNO injection and saline injection in the DREADDs-expressing group. In this analysis, fALFF values were extracted from voxels in a mask consisting of the mean group FC map of seed regions in the right Cg and right RSP (see Figures 3E–3H). These seed regions are key nodes of the DMLN in rats, and their FC maps were used as estimated masks of the DMLN FC. The obtained masks were divided into unilateral masks for the ipsilateral right hemisphere and for the contralateral left hemisphere. The extracted fALFF values in the masks of the right DMLN showed significant decreases (Figure 3H). Interestingly, no alterations were observed in the fALFF values from the maps in the left hemisphere (Figure 3G).

Right BFB Stimulation Does Not Alter FC and Resting-State Neural Activity in the Task-Positive Network

To investigate if the changes observed in FC and neural activity observed in the DMLN are also present in other resting-state networks (RSNs), we also analyzed the TPN, which in rats includes somatosensory, motor, and insular cortices. No significant differences were observed after injection of saline versus CNO in an ROI-based analysis (Figure 4A). Moreover, investigation of the low-frequency neural activity using fALFF demonstrates no significant differences in neural activity in the TPN after injection of saline or CNO (Figure 4B). These results suggest that the observed changes in FC upon activation of cholinergic neurons in the right basal forebrain are specific to the DMLN.

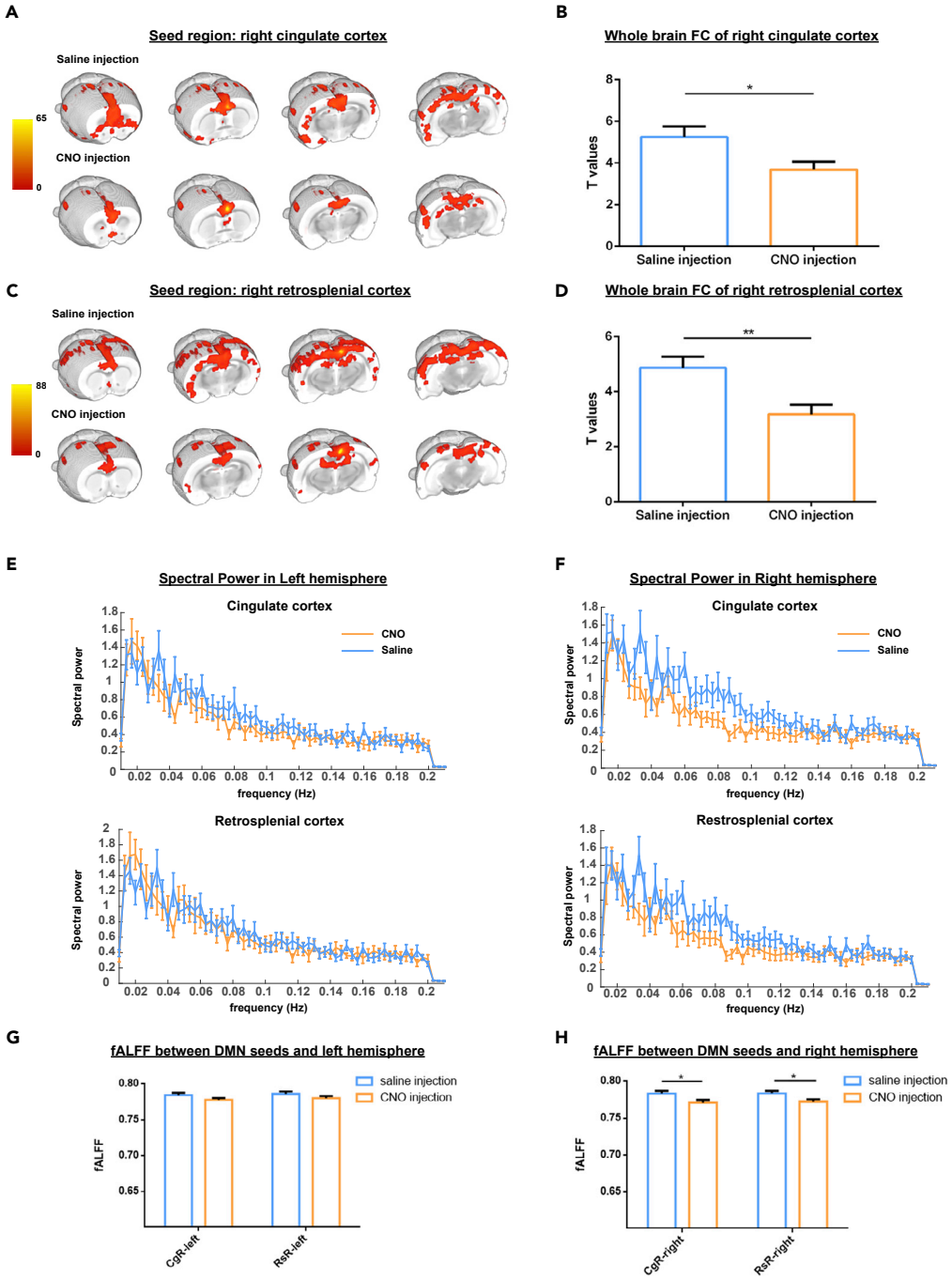

Figure 3. Right Basal Forebrain (BFB) Stimulation Induces Functional Connectivity and Resting-State Neural Activity Decreases in the Default Mode like network (DMLN)

(A and C) Representation of mean seed-based FC maps of the right cingulate cortex (A) and right retrosplenial cortex (C) in the DREADDs-expressing group after injection of saline and CNO (one-sample t test, FWE corrected $p \leq 0.05$, minimal cluster size = 10 voxels).

(B and D) Quantification of the FC strength as mean t values ± SEM for both seed regions (right cingulate cortex (B) and right retrosplenial cortex (D)). Statistical comparisons were performed using a paired Student's t test.

(E and F) Group-averaged power-spectra of the seed-based maps of the cingulate and retrosplenial cortex in the left (E) and right (F) hemispheres. Blue curves are the power spectra after injection of saline, orange curves are the power spectra after injection of CNO.

Figure 3. *Continued*
(G and H) fALFF values calculated from the seed-based FC maps of the right cingulate cortex and right retrosplenial cortex. fALFF values were extracted from voxels of the left hemisphere (G) and right hemisphere (H), after saline injection (blue) and CNO injection (orange). The bar graphs present mean fALFF values ±SEM. A paired Student's t test was used to statistically compare the mean fALFF values between saline injection and CNO injection within the same group. *$p \leq 0.05$, **$p \leq 0.01$. Abbreviations: FC, functional connectivity; DMLN, default mode like network; fALFF, fractional amplitude of low frequency fluctuations.

Unilateral Stimulation of Right BFB Induces Lateralized Effects in DMLN and TPN

In the current study, DREADDs were injected in the right basal forebrain during a stereotactic surgery. To evaluate the successful unilateral expression of the DREADDs, histological analysis of the m-Cherry expression in the BFB of both hemispheres was performed in a subset of animals (N = 2). The percentage area of m-Cherry as well as the mean intensities in the maximum-intensity projection were calculated and normalized according to the percentage area and mean intensity of DAPI. Then, the expression laterality index (ELI) was calculated using ELI=(R-L)/(R + L) for each of the two animals. Figure 5A demonstrates that the m-Cherry expression was highly localized to the right basal forebrain, with only minor m-Cherry present in the side contralateral to the injection site leading to expression laterality indices greater than 0.98 for both animals. Then, according to our hypothesis, we investigated if the unilateral stimulation of neurons in the right basal forebrain expressing DREADDS would induce asymmetric and lateralized changes in FC. To evaluate this, connectivity laterality indices (CLIs) were calculated based on the ROI-based matrices of the DMLN and TPN, as described previously by Di et al. (2014). Comparison of the CLI after injection of CNO and saline revealed a significant increase in CLI toward the left hemisphere (as expected from decreased FC in the right hemisphere) for a specific DMN pair and, namely, the connection between ORF and PtPD (paired t test, FDR-corrected (0.05); $p = 0.0026$). Interestingly, although no significant changes in global FC were observed in the TPN, analysis of the laterality revealed a shift toward the left hemisphere for some connections upon cholinergic activation (Figure 5B).

DISCUSSION

Chemogenetic-fMRI can provide important information about the effects of particular nodes in the brain on whole brain activity and connectivity within specific networks (Giorgi et al., 2017; Peeters et al., 2020). In this study, excitatory DREADDs were expressed in the right BFB cholinergic neurons of rats and the effects of DREADDs-induced neural activity alterations were evaluated by means of non-invasive rsfMRI. Several studies have already highlighted that the combination of the DREADDs technology and *in vivo* imaging techniques is an emerging powerful tool allowing scientists to advance their knowledge of brain networks in health and disease (reviewed in Peeters et al., 2019). Here, the excitatory DREADDs in the right BFB cholinergic neurons were activated by CNO injection and rsfMRI scans were acquired to evaluate the effect on FC and resting-state neural activity in brain regions of the DMLN. We showed that the effects of CNO-induced stimulation of BFB cholinergic neurons appear at 5–10 min after administration. The temporal evolution of FC changes we observed is consistent with previous research that demonstrated DREADDs-induced neural activity modulations starting at 5 min after administration of its ligand CNO (Alexander et al., 2009; Roelofs et al., 2017). Analysis of the CNO-induced functional connectivity and fALFF changes indicated a general unilateral decrease in FC and fALFF values in the DMLN ipsilateral to the expression cite in the BFB, whereas changes in other networks were not significant. Notably, significant connectivity laterality changes were found both in the DMN and TPN networks indicating that unilateral BFB cholinergic stimulation can induce brain state changes consistent with a biased attentional processing toward the ipsilateral hemisphere. Importantly, control experiments with CNO injections in sham animals demonstrated the absence of non-specific effects.

The DMN is implicated in higher cognitive functions that are thought to be specific for humans, such as mind wandering and thinking about the past and future. The discovery of a DMLN present in rodents raises questions about the functional homology between these networks. Moreover, the need for anesthetics and the differences in anatomy between humans and rodents further impede interpretation and translation. Previously, we have shown that visual stimulation decreases FC and deactivates nodes of the DMLN in rats (Hinz et al., 2019), similar to observations in humans (Razlighi, 2018). Several studies have demonstrated that pharmacological stimulation of the human cholinergic system induces a desynchronization in the DMN (reviewed in Sutherland et al., 2015), which is analogous with the observations in this study. The aforementioned observations thus suggest shared mechanisms of task-induced DMN suppression across species.

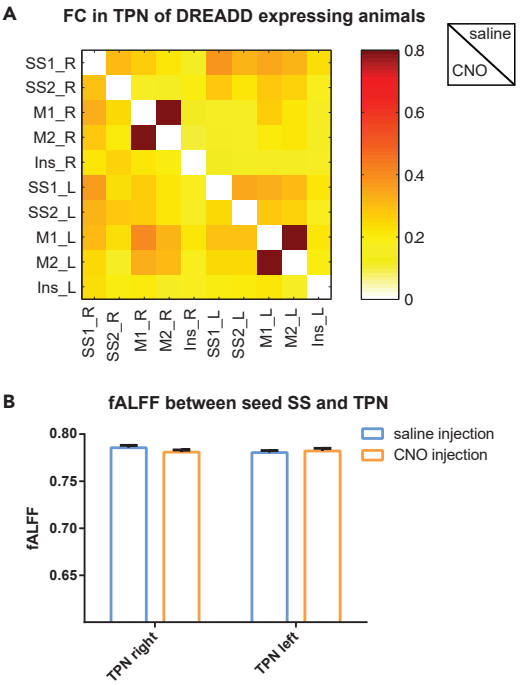

Figure 4. DREADDs-Induced Right Basal Forebrain (BFB) Stimulation Does Not Induce Changes in Functional Connectivity and Neural Activity in the Task-Positive Network (TPN)

(A) Pairwise z-transformed FC matrix after saline injection (sub-diagonal) and after CNO injection (supra-diagonal) in the DREADDs-expressing group. The color bar represents *Z* scores. No significant differences were observed between the two conditions (repeated measures two-way ANOVA with Sidak's correction for multiple comparisons).

(B) fALFF values calculated from the seed-based FC maps of the left and right primary somatosensory cortex. fALFF values were extracted from voxels of the left hemisphere and right hemisphere, after saline injection (blue) and CNO injection (orange). The bar graphs present mean fALFF values ± SEM. A paired Student's t test was used to statistically compare the mean fALFF values between saline injection and CNO injection. Abbreviations: SS1, primary somatosensory cortex; SS2, secondary somatosensory cortex; M1, primary motor cortex; M2, secondary motor cortex; Ins, insular cortex; TPN, task-positive network.

The BFB contains prominent groups of cholinergic, GABAergic, and glutamatergic neurons through which it can modulate the entire neocortex. In a recent study, Turchi et al. (2018) investigated how neuronal populations in the BFB contribute to the spontaneous fMRI fluctuations in the cerebral cortex of monkeys. The authors demonstrated that unilateral inactivation of the BFB, in particular the nucleus basalis of Meynert, induced a prominent ipsilateral decrease in the global component of the spontaneous fMRI fluctuations across its cortical projection areas. Furthermore, the spatial extent of commonly observed resting-state networks remained unaltered, whereas significant decreases in ipsilateral network strength could be observed (Turchi et al., 2018). Those results support the neuromodulatory role of the basal forebrain via its control of global spontaneous fluctuations. Advancing further than the above-described results, our study shows that unilateral stimulation specific to the cholinergic BFB system induces mainly ipsilateral FC reductions in the DMLN. Moreover, in our study, selective activation of cholinergic neurons could produce differential effects between the DMN and other networks, suggesting that specificity can play an important role in the surge for therapies targeting specific networks, which provides a specific manipulation tool for both fundamental studies of neuromodulation as well as potential rehabilitation efforts in disorders with lateralized attentional deficits such as hemispatial neglect.

Previous tract tracing studies revealed that the cholinergic BFB neurons collectively project toward a broad range of cortical areas as well as to brain regions of the limbic system and thalamic nuclei (Mesulam et al., 1983). It has been shown that these cholinergic projection neurons are driven by differential inputs allowing control of the efflux of acetylcholine and its timescale in various brain regions (Gielow and Zaborszky, 2017). This supports the role of the BFB in various networks that are implicated in, for example, attentional processes (Gielow and Zaborszky, 2017; Sarter et al., 2001). As such, several behavioral and neuroimaging studies provided evidence suggesting that attentional processes, including "top-down" and "bottom-up" processes, depend on intact BFB cholinergic corticopetal projections (Pinto et al., 2013; Sarter et al., 2001).

The connections between the BFB and PFC have been implicated in the regulation of the DMN (Nair et al., 2018; Alves et al., 2019). In 2018, Nair et al. demonstrated that the BFB exhibits local gamma oscillations that influence gamma-band activity in a hub region of the DMLN, the anterior cingulate cortex, during rest (Nair et al., 2018). In humans, gamma-band activity in DMN areas is elevated during periods of quiet wakefulness and is transiently suppressed during the performance of cognitive tasks (Miller et al., 2009; Ossandon et al., 2011). It has been suggested that GABAergic cells, in particular somatostatin-

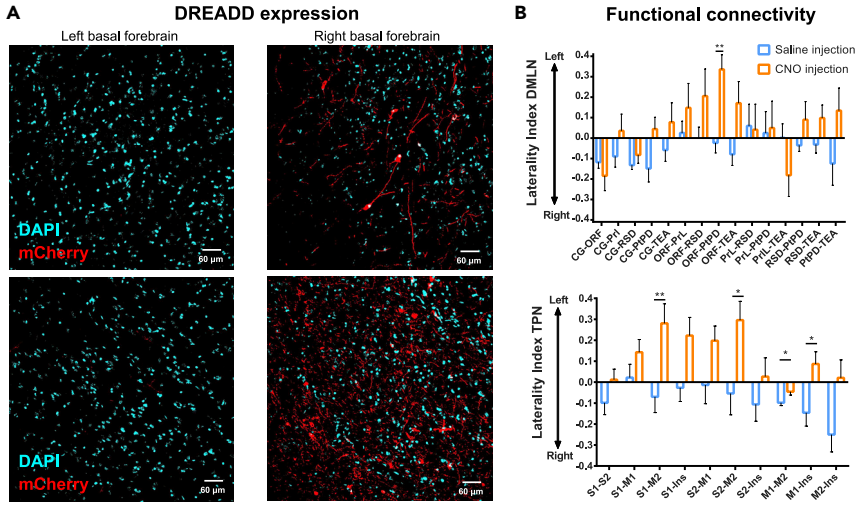

Figure 5. Lateralized Expression of DREADDs in the Basal Forebrain Induces Lateralized Changes in FC in DMLN and TPN

(A) Maximum-intensity projections of the left and right basal forebrain of two DREADD-expressing animals were obtained and were thresholded, after which the area percentage of m-Cherry and DAPI was calculated. Next, the area percentage and mean intensity of the m-Cherry were normalized to the DAPI and an expression laterality index (ELI) was calculated. The images demonstrate a highly lateralized expression of m-Cherry, predominantly in the right hemisphere (0.99 top pair, 0.98 bottom pair).

(B) Connectivity laterality indices (CLI) were calculated for each ROI pair in the DMLN (top panel) and TPN (bottom panel). Bar graphs represent the mean CLI ± SEM, with negative values indicating right hemispheric dominance, whereas positive values indicate left hemispheric dominance. Paired Student's t test was used to statistically compare the mean CLI between saline injection and CNO injection. *$p \leq 0.05$, **$p \leq 0.01$. Abbreviations: DREADDs, designer receptors exclusively activated by designer drugs; Cg, cingulate cortex; ORB, orbitofrontal cortex; PrL, prelimbic cortex; RS, retrosplenial cortex; PtPD, parietal association cortex; TEA, temporal association cortex; FC, functional connectivity; DMLN, default mode like network; CNO, clozapine-N-oxide; SS1, primary somatosensory cortex; SS2, secondary somatosensory cortex; M1, primary motor cortex; M2, secondary motor cortex; Ins, insular cortex; TPN, task-positive network.

expressing cells, or the glutamatergic cells in the BFB mediate the generation and coordination of these gamma oscillations (Espinosa et al., 2019a, 2019b; Yang et al., 2017). In our study, analysis of the low-frequency fluctuations in the BOLD signal revealed decreased FC and resting-state neural activity in cortical DMLN region upon stimulation of BFB cholinergic neurons. Interestingly, the low-frequency fluctuations in the BOLD signal have been suggested to be related to spontaneous gamma band local field potentials (Leopold et al., 2003). Therefore, decreases in FC and resting-state neural activity (measured by fALFF) might be related to decreased activity in neurons giving rise to gamma oscillations, such as GABAergic and glutamatergic BFB neurons. We suggest that our findings might be mediated through local axonal collaterals from BFB cholinergic neurons that terminate on other BFB cell types (Zaborszky and Duque, 2000). This is in line with other studies showing that the connections between cholinergic neurons and somatostatin cells in the BFB are antagonistic (Xu et al., 2015; Zaborszky and Duque, 2000). Additionally, cholinergic stimulation can induce inhibition of the BFB glutamatergic neurons (Yang et al., 2017). The latter is thought to exert its effect on the DMN via the ventral striatum (van der Meer et al., 2010). The interactions between both neuronal populations and the cholinergic neurons might be an underlying mechanism through which the attention networks and DMN exert their antagonism. However, future investigations of the BFB-DMN circuitry have to be performed in order to elucidate the contributions of specific BFB cell types.

Increases in cholinergic tone have been observed in rats performing a visual attention task (Parikh et al., 2007). Pinto et al. (2013) showed that enhanced acetylcholine levels, by stimulation of the BFB cholinergic neurons, can improve visual discrimination and sensory processing by inducing desynchronization of cortical activity (Pinto et al., 2013). Recently, we showed that stimulating bottom-up sensory processing in sedated rats induced decreases in FC between different nodes of the DMLN (Hinz et al., 2019).

Collectively, these findings might suggest involvement of the BFB cholinergic system in mediating the reduced FC in the DMLN upon stimulation of bottom-up sensory processes.

Previous studies suggested that the basal forebrain is a key player in modulation of cortical networks. In this study, we combined the DREADD technology with *in vivo* MRI in rats in order to explore the involvement of the BFB cholinergic system in the regulation of the DMLN. As such, excitatory DREADDs were used to selectively activate cholinergic neurons in the right BFB and resting-state fMRI scans were acquired to evaluate the effect on DMLN FC and resting-state neural activity. This is the first study that demonstrates decreased right intra- and interhemispheric FC in the DMLN as well as decreased right intra-hemispheric resting-state neural activity upon selective, cholinergic stimulation, in sedated rats. We conjecture that our DREADDs-induced stimulation of the BFB cholinergic neurons mediates decreased DMLN FC through similar pathways as task-related DMLN suppression. To conclude, our findings enrich the current understanding of the DMLN and its underlying mechanisms in rodents and provide a specific tool for future manipulation of activity and connectivity in studies interested in cholinergic neuromodulation both in health and disease.

LIMITATIONS OF THE STUDY

Despite DREADDs being an exquisite tool allowing specific targeting of neuronal populations, their temporal precision is limited owing to the systemic nature of their application and the mechanisms of action (most via G-protein-coupled receptors). In contrast, optogenetics, a technique that allows similar specificity, allows manipulation of cell activities with millisecond precision and recent advancements provide single cell precision, albeit at the cost of more invasive manipulations. Several studies have shown that acute versus tonic cholinergic stimulation induce different effects. Therefore, diverging results could be obtained when combining optogenetics with rsfMRI. Both techniques are still developing, and thus some of these limitations are expected to get eliminated in the future. Another limitation of our study is that, although we targeted specifically the cholinergic cells the effects could be mediated through interactions between other neuronal populations in the basal forebrain. More experiments investigating the local interactions of the different neuronal populations in the BFB would be valuable to further elucidate the neuronal mechanisms underlying the neuromodulatory effects of the cholinergic system on the DMLN. To conclude, in the current study, only the right BFB was transfected with DREADDs, resulting in a lateralized decrease in FC in the DMLN. It would be interesting to compare these results with the effects of a bilateral cholinergic stimulation.

Resource Availability

Lead Contact

Further information and requests for resources and data should be directed to and will be fulfilled by the Lead Contact, Georgios A. Keliris (georgios.keliris@uantwerpen.be).

Materials Availability

The study did not generate new unique agents.

Data and Code Availability

The complete MRI dataset generated during this study are available at Xnat Central: [central.xnat.org - code: DMLN].

The histological data are available at Mendeley Data: https://doi.org/10.17632/ckr89fwd5w.1.

METHODS

All methods can be found in the accompanying Transparent Methods supplemental file.

SUPPLEMENTAL INFORMATION

Supplemental Information can be found online at https://doi.org/10.1016/j.isci.2020.101455.

ACKNOWLEDGMENTS

This study was supported by the Fund of Scientific Research Flanders (FWO G048917N) and the University Research Fund of University of Antwerp (BOF DOCPRO FFB150340). The Leica SP 8 (Hercules grant AUHA.15.12) microscope was funded by the Hercules Foundation of the Flemish Government. The computational resources and services used in this work were provided by the HPC core facility CalcUA of the University of Antwerp, the VSC (Flemish Supercomputer Center), funded by the Hercules Foundation and the Flemish Government – department EWI.

AUTHOR CONTRIBUTIONS

L.M.P., M.v.d.B., and G.A.K. designed the study. L.M.P. and M.v.d.B. performed the stereotactic surgeries and MRI experiments. L.M.P., M.v.d.B., and G.A.K. performed the MRI data analysis and interpretation. L.M.P. and M.v.d.B. optimized and performed the immunofluorescent staining under the guidance of G.M. I.P., L.M.P., and M.v.d.B. acquired the microscopy images shown in Figures 1 and 5 of this manuscript. L.M.P., M.v.d.B., and G.A.K. wrote the manuscript. G.A.K. supervised the study and supported the study with equipment and materials. All co-authors provided comments and intellectual input that led to the final version of the manuscript.

DECLARATION OF INTERESTS

The authors declare no competing interests.

Received: April 16, 2020
Revised: July 14, 2020
Accepted: August 10, 2020
Published: September 25, 2020

REFERENCES

Alexander, G.M., Rogan, S.C., Abbas, A.I., Armbruster, B.N., Pei, Y., Allen, J.A., Nonneman, R.J., Hartmann, J., Moy, S.S., Nicolelis, M.A., et al. (2009). Remote control of neuronal activity in transgenic mice expressing evolved G protein-coupled receptors. Neuron *63*, 27–39.

Alves, P.N., Foulon, C., Karolis, V., Bzdok, D., Margulies, D.S., Volle, E., and Thiebaut de Schotten, M. (2019). An improved neuroanatomical model of the default-mode network reconciles previous neuroimaging and neuropathological findings. Commun. Biol. *2*, 370.

Anckaerts, C., Blockx, I., Summer, P., Michael, J., Hamaide, J., Kreutzer, C., Boutin, H., Couillard-Despres, S., Verhoye, M., and van der Linden, A. (2019). Early functional connectivity deficits and progressive microstructural alterations in the TgF344-AD rat model of Alzheimer's Disease: a longitudinal MRI study. Neurobiol. Dis. *124*, 93–107.

Andrews-Hanna, J.R., Reidler, J.S., Huang, C., and Buckner, R.L. (2010). Evidence for the default network's role in spontaneous cognition. J. Neurophysiol. *104*, 322–335.

Ballinger, E.C., Ananth, M., Talmage, D.A., and Role, L.W. (2016). Basal forebrain cholinergic circuits and signaling in cognition and cognitive decline. Neuron *91*, 1199–1218.

Bartolomeo, P., Thiebaut de Schotten, M., and Chica, A.B. (2012). Brain networks of visuospatial attention and their disruption in visual neglect. Front. Hum. Neurosci. *6*, 110.

Belloy, M.E., Naeyaert, M., Abbas, A., Shah, D., Vanreusel, V., van Audekerke, J., Keilholz, S.D., KELIRIS, G.A., van der Linden, A., and Verhoye, M. (2018). Dynamic resting state fMRI analysis in mice reveals a set of Quasi-Periodic Patterns and illustrates their relationship with the global signal. Neuroimage *180*, 463–484.

Bloem, B., Schoppink, L., Rotaru, D.C., Faiz, A., Hendriks, P., Mansvelder, H.D., van de Berg, W.D., and Wouterlood, F.G. (2014). Topographic mapping between basal forebrain cholinergic neurons and the medial prefrontal cortex in mice. J. Neurosci. *34*, 16234–16246.

Broyd, S.J., Demanuele, C., Debener, S., Helps, S.K., James, C.J., and Sonuga-Barke, E.J. (2009). Default-mode brain dysfunction in mental disorders: a systematic review. Neurosci. Biobehav Rev. *33*, 279–296.

Buckner, R.L., and Carroll, D.C. (2007). Self-projection and the brain. Trends Cogn. Sci. *11*, 49–57.

Buckner, R.L., and Dinicola, L.M. (2019). The brain's default network: updated anatomy, physiology and evolving insights. Nat. Rev. Neurosci. *20*, 593–608.

Chaves-Coira, I., Martin-Cortecero, J., Nunez, A., and Rodrigo-Angulo, M.L. (2018). Basal forebrain nuclei display distinct projecting pathways and functional circuits to sensory primary and prefrontal cortices in the rat. Front. Neuroanat. *12*, 69.

Chen, N., Sugihara, H., and Sur, M. (2015). An acetylcholine-activated microcircuit drives temporal dynamics of cortical activity. Nat. Neurosci. *18*, 892–902.

Di, X., Kim, E.H., Chen, P., and Biswal, B.B. (2014). Lateralized resting-state functional connectivity in the task-positive and task-negative networks. Brain Connect. *4*, 641–648.

Espinosa, N., Alonso, A., Lara-Vasquez, A., and Fuentealba, P. (2019a). Basal forebrain somatostatin cells differentially regulate local gamma oscillations and functionally segregate motor and cognitive circuits. Sci. Rep. *9*, 2570.

Espinosa, N., Alonso, A., Morales, C., Espinosa, P., Chavez, A.E., and Fuentealba, P. (2019b). Basal forebrain gating by somatostatin neurons drives prefrontal cortical activity. Cereb. Cortex *29*, 42–53.

Fox, M.D., Snyder, A.Z., Vincent, J.L., Corbetta, M., van Essen, D.C., and Raichle, M.E. (2005). The human brain is intrinsically organized into dynamic, anticorrelated functional networks. Proc. Natl. Acad. Sci. U S A *102*, 9673–9678.

Fransson, P. (2006). How default is the default mode of brain function? Further evidence from intrinsic BOLD signal fluctuations. Neuropsychologia *44*, 2836–2845.

Gao, W., Gilmore, J.H., Alcauter, S., and Lin, W. (2013). The dynamic reorganization of the default-mode network during a visual classification task. Front. Syst. Neurosci. *7*, 34.

Gielow, M.R., and Zaborszky, L. (2017). The input-output relationship of the cholinergic basal forebrain. Cell Rep. *18*, 1817–1830.

Giorgi, A., Migliarini, S., Galbusera, A., Maddaloni, G., Mereu, M., Margiani, G., Gritti, M., Landi, S., Trovato, F., Bertozzi, S.M., et al. (2017). Brain-wide mapping of endogenous serotonergic transmission via chemogenetic fMRI. Cell Rep. *21*, 910–918.

Greicius, M.D., Flores, B.H., Menon, V., Glover, G.H., Solvason, H.B., Kenna, H., Reiss, A.L., and Schatzberg, A.F. (2007). Resting-state functional connectivity in major depression: abnormally increased contributions from subgenual cingulate cortex and thalamus. Biol. Psychiatry *62*, 429–437.

Greicius, M.D., Krasnow, B., Reiss, A.L., and Menon, V. (2003). Functional connectivity in the resting brain: a network analysis of the default mode hypothesis. Proc. Natl. Acad. Sci. U S A. *100*, 253–258.

Greicius, M.D., Srivastava, G., Reiss, A.L., and Menon, V. (2004). Default-mode network activity distinguishes Alzheimer's disease from healthy aging: evidence from functional MRI. Proc. Natl. Acad. Sci. U S A *101*, 4637–4642.

Gritton, H.J., Howe, W.M., Mallory, C.S., Hetrick, V.L., Berke, J.D., and Sarter, M. (2016). Cortical cholinergic signaling controls the detection of cues. Proc. Natl. Acad. Sci. U S A *113*, E1089–E1097.

Hinz, R., Peeters, L.M., Shah, D., Missault, S., Belloy, M., Vanreusel, V., Malekzadeh, M., Verhoye, M., van der Linden, A., and Keliris, G.A. (2019). Bottom-up sensory processing can induce negative BOLD responses and reduce functional connectivity in nodes of the default mode-like network in rats. Neuroimage *197*, 167–176.

Howe, W.M., Gritton, H.J., Lusk, N.A., Roberts, E.A., Hetrick, V.L., Berke, J.D., and Sarter, M. (2017). Acetylcholine release in prefrontal cortex promotes gamma oscillations and theta-gamma coupling during cue detection. J. Neurosci. *37*, 3215–3230.

Laufs, H., Hamandi, K., Salek-Haddadi, A., Kleinschmidt, A.K., Duncan, J.S., and Lemieux, L. (2007). Temporal lobe interictal epileptic discharges affect cerebral activity in "default mode" brain regions. Hum. Brain Mapp. *28*, 1023–1032.

Leopold, D.A., Murayama, Y., and Logothetis, N.K. (2003). Very slow activity fluctuations in monkey visual cortex: implications for functional brain imaging. Cereb. Cortex *13*, 422–433.

Li, W., Motelow, J.E., Zhan, Q., Hu, Y.C., Kim, R., Chen, W.C., and Blumenfeld, H. (2015). Cortical network switching: possible role of the lateral septum and cholinergic arousal. Brain Stimul. *8*, 36–41.

Lu, H., Zou, Q., Gu, H., Raichle, M.E., Stein, E.A., and Yang, Y. (2012). Rat brains also have a default mode network. Proc. Natl. Acad. Sci. U S A *109*, 3979–3984.

Mayer, J.S., Roebroeck, A., Maurer, K., and Linden, D.E. (2010). Specialization in the default mode: task-induced brain deactivations dissociate between visual working memory and attention. Hum. Brain Mapp. *31*, 126–139.

Mesulam, M.M., Mufson, E.J., Wainer, B.H., and Levey, A.I. (1983). Central cholinergic pathways in the rat: an overview based on an alternative nomenclature (Ch1-Ch6). Neuroscience *10*, 1185–1201.

Miller, K.J., Weaver, K.E., and Ojemann, J.G. (2009). Direct electrophysiological measurement of human default network areas. Proc. Natl. Acad. Sci. U S A *106*, 12174–12177.

Nair, J., Klaassen, A.L., Arato, J., Vyssotski, A.L., Harvey, M., and Rainer, G. (2018). Basal forebrain contributes to default mode network regulation. Proc. Natl. Acad. Sci. U S A *115*, 1352–1357.

Nguyen, H.N., Huppe-Gourgues, F., and Vaucher, E. (2015). Activation of the mouse primary visual cortex by medial prefrontal subregion stimulation is not mediated by cholinergic basalo-cortical projections. Front. Syst. Neurosci. *9*, 1.

Ossandon, T., Jerbi, K., Vidal, J.R., Bayle, D.J., Henaff, M.A., Jung, J., Minotti, L., Bertrand, O., Kahane, P., and Lachaux, J.P. (2011). Transient suppression of broadband gamma power in the default-mode network is correlated with task complexity and subject performance. J. Neurosci. *31*, 14521–14530.

Parikh, V., Kozak, R., Martinez, V., and Sarter, M. (2007). Prefrontal acetylcholine release controls cue detection on multiple timescales. Neuron *56*, 141–154.

Peeters, L.M., Hinz, R., Detrez, J.R., Missault, S., de Vos, W.H., Verhoye, M., van der Linden, A., and Keliris, G.A. (2020). Chemogenetic silencing of neurons in the mouse anterior cingulate area modulates neuronal activity and functional connectivity. Neuroimage *220*, 117088.

Peeters, L.M., Missault, S., Keliris, A.J., and Keliris, G.A. (2019). Combining DREADDs and neuroimaging in experimental models: a powerful approach towards neurotheranostic applications. Br. J. Pharmacol. *177*, 992–1002.

Pinto, L., Goard, M.J., Estandian, D., Xu, M., Kwan, A.C., Lee, S.H., Harrison, T.C., Feng, G., and Dan, Y. (2013). Fast modulation of visual perception by basal forebrain cholinergic neurons. Nat. Neurosci. *16*, 1857–1863.

Raichle, M.E., Macleod, A.M., Snyder, A.Z., Powers, W.J., Gusnard, D.A., and Shulman, G.L. (2001). A default mode of brain function. Proc. Natl. Acad. Sci. U S A. *98*, 676–682.

Raichle, M.E., and Snyder, A.Z. (2007). A default mode of brain function: a brief history of an evolving idea. Neuroimage *37*, 1083–1090, discussion 1097-9.

Rajan, A., Meyyappan, S., Walker, H., Henry Samuel, I.B., Hu, Z., and Ding, M. (2019). Neural mechanisms of internal distraction suppression in visual attention. Cortex *117*, 77–88.

Razlighi, Q.R. (2018). Task-evoked negative BOLD response in the default mode network Does not alter its functional connectivity. Front. Comput. Neurosci. *12*, 67.

Roelofs, T.J.M., Verharen, J.P.H., van Tilborg, G.A.F., Boekhoudt, L., van Der Toorn, A., de Jong, J.W., Luijendijk, M.C.M., Otte, W.M., Adan, R.A.H., and Dijkhuizen, R.M. (2017). A novel approach to map induced activation of neuronal networks using chemogenetics and functional neuroimaging in rats: a proof-of-concept study on the mesocorticolimbic system. Neuroimage *156*, 109–118.

Rohleder, C., Wiedermann, D., Neumaier, B., Drzezga, A., Timmermann, L., Graf, R., Leweke, F.M., and Endepols, H. (2016). The functional networks of prepulse inhibition: neuronal connectivity analysis based on FDG-PET in awake and unrestrained rats. Front. Behav. Neurosci. *10*, 148.

Sarter, M., Givens, B., and Bruno, J.P. (2001). The cognitive neuroscience of sustained attention: where top-down meets bottom-up. Brain Res. Brain Res. Rev. *35*, 146–160.

Schwarz, A.J., Gass, N., Sartorius, A., Risterucci, C., Spedding, M., Schenker, E., Meyer-Lindenberg, A., and Weber-Fahr, W. (2013). Anti-correlated cortical networks of intrinsic connectivity in the rat brain. Brain Connect. *3*, 503–511.

Sforazzini, F., Bertero, A., Dodero, L., David, G., Galbusera, A., Scattoni, M.L., Pasqualetti, M., and Gozzi, A. (2016). Altered functional connectivity networks in acallosal and socially impaired BTBR mice. Brain Struct. Funct. *221*, 941–954.

Shah, D., Praet, J., Latif Hernandez, A., Hofling, C., Anckaerts, C., Bard, F., Morawski, M., Detrez, J.R., Prinsen, E., Villa, A., et al. (2016). Early pathologic amyloid induces hypersynchrony of BOLD resting-state networks in transgenic mice and provides an early therapeutic window before amyloid plaque deposition. Alzheimers Dement. *12*, 964–976.

Shulman, G.L., Fiez, J.A., Corbetta, M., Buckner, R.L., Miezin, F.M., Raichle, M.E., and Petersen, S.E. (1997). Common blood flow changes across visual tasks: II. Decreases in cerebral cortex. J. Cogn. Neurosci. *9*, 648–663.

Singh, K.D., and Fawcett, I.P. (2008). Transient and linearly graded deactivation of the human default-mode network by a visual detection task. Neuroimage *41*, 100–112.

Stafford, J.M., Jarrett, B.R., Miranda-Dominguez, O., Mills, B.D., Cain, N., Mihalas, S., Lahvis, G.P., Lattal, K.M., Mitchell, S.H., David, S.V., et al. (2014). Large-scale topology and the default mode network in the mouse connectome. Proc. Natl. Acad. Sci. U S A *111*, 18745–18750.

Sutherland, M.T., Ray, K.L., Riedel, M.C., Yanes, J.A., Stein, E.A., and Laird, A.R. (2015). Neurobiological impact of nicotinic acetylcholine receptor agonists: an activation likelihood estimation meta-analysis of pharmacologic neuroimaging studies. Biol. Psychiatry *78*, 711–720.

Tian, L., Jiang, T., Wang, Y., Zang, Y., He, Y., Liang, M., Sui, M., Cao, Q., Hu, S., Peng, M., and Zhuo, Y. (2006). Altered resting-state functional connectivity patterns of anterior cingulate cortex in adolescents with attention deficit hyperactivity disorder. Neurosci. Lett. *400*, 39–43.

Turchi, J., Chang, C., Ye, F.Q., Russ, B.E., Yu, D.K., Cortes, C.R., Monosov, I.E., Duyn, J.H., and Leopold, D.A. (2018). The basal forebrain regulates global resting-state fMRI fluctuations. Neuron *97*, 940–952 e4.

van der Meer, M.A., Kalenscher, T., Lansink, C.S., Pennartz, C.M., Berke, J.D., and Redish, A.D. (2010). Integrating early results on ventral striatal gamma oscillations in the rat. Front. Neurosci. *4*, 300.

Vincent, J.L., Patel, G.H., Fox, M.D., Snyder, A.Z., Baker, J.T., van Essen, D.C., Zempel, J.M., Snyder, L.H., Corbetta, M., and Raichle, M.E. (2007). Intrinsic functional architecture in the anaesthetized monkey brain. Nature *447*, 83–86.

Wen, X., Liu, Y., Yao, L., and Ding, M. (2013). Top-down regulation of default mode activity in spatial visual attention. J. Neurosci. *33*, 6444–6453.

Witten, I.B., Steinberg, E.E., Lee, S.Y., Davidson, T.J., Zalocusky, K.A., Brodsky, M., Yizhar, O., Cho, S.L., Gong, S., Ramakrishnan, C., et al. (2011). Recombinase-driver rat lines: tools, techniques, and optogenetic application to dopamine-mediated reinforcement. Neuron *72*, 721–733.

Xu, M., Chung, S., Zhang, S., Zhong, P., Ma, C., Chang, W.C., Weissbourd, B., Sakai, N., Luo, L., Nishino, S., and Dan, Y. (2015). Basal forebrain circuit for sleep-wake control. Nat. Neurosci. *18*, 1641–1647.

Yang, C., Mckenna, J.T., and Brown, R.E. (2017). Intrinsic membrane properties and cholinergic modulation of mouse basal forebrain glutamatergic neurons in vitro. Neuroscience *352*, 249–261.

Zaborszky, L., and Duque, A. (2000). Local synaptic connections of basal forebrain neurons. Behav. Brain Res. *115*, 143–158.

Zou, Q.H., Zhu, C.Z., Yang, Y., Zuo, X.N., Long, X.Y., Cao, Q.J., Wang, Y.F., and Zang, Y.F. (2008). An improved approach to detection of amplitude of low-frequency fluctuation (ALFF) for resting-state fMRI: fractional ALFF. J. Neurosci. Methods *172*, 137–141.

iScience, Volume *23*

Supplemental Information

Cholinergic Modulation of the Default Mode Like Network in Rats

Lore M. Peeters, Monica van den Berg, Rukun Hinz, Gaurav Majumdar, Isabel Pintelon, and Georgios A. Keliris

Supplemental information

1. Transparent methods

1.1 Animals and ethical statement

In this study, 28 adult ChAT-Cre Long Evans rats were used, of which 14 males and 14 females. Animals were group housed with a 12h light/dark cycle and with controlled temperature (20 – 24°C) and humidity (40%) conditions. Standard food and water were provided ad libitum. All procedures were in accordance with the guidelines approved by the European Ethics Committee (decree 2010/63/EU) and were approved by the Committee on Animal Care and Use at the University of Antwerp, Belgium (approval number: 2015-50).

1.2 Intracerebral viral vector injections

The rats were divided in a control group (N = 12) and an experimental group (N = 16) with DREADDs expression. All rats were subjected to a stereotactic surgery targeting the medial nuclei of the right basal forebrain (BFB), ie the horizontal diagonal band of Broca, nucleus basalis of Meynert and the substantia innominata (AP = -0.5 mm, ML = +2.5mm, DV= -7.5mm from bregma). The stereotactic surgery was performed as follows: rats were anesthetized using 5% isoflurane for induction and 2% for maintenance (Isoflo®, Abbott Laboratories, Ltd., USA) and received a subcutaneous injection of xylocaine (Lidocaine hydrochloride, Astra Zeneca) for local analgesia. The rats received a unilateral injection with a Cre-dependent AAV-virus: AAV8-hSyn-DIO-hM3Dq(Gq)-mCherry (4.8 x 10^{12} GC/mL) for the experimental group and AAV8-hSyn-DIO-mCherry (4.1 x 10^{12} GC/mL) for the control group. Chat-cre transgenic rats were used to specifically express the DREADDs receptors in all cholinergic neurons in the right BFB. A glass pipette filled with 2.5 µL of the viral vectors was used to inject 2 µL in the brain region of interest at a rate of 46 nL/min using a nano-injector (Nanoject II, Drummond Scientific). At ten minutes after the viral vector injection, the glass pipet was removed from the brain tissue. All MRI procedures started at least two months after viral vector injection to allow full recovery and optimal expression levels of the DREADDs receptors (Urban et al., 2016).

1.3 In vivo MRI procedures

At the start of the MRI scanning procedures, the rats were anesthetized using isoflurane (5% for induction and 2% for handling procedures). After fixation of the animal in the scanner, the isoflurane was gradually lowered to 0.4 % and an intravenous bolus injection of medetomidine (0.05 mg/kg, Domitor®, Pfizer, Germany) was administered. At 15 minutes after the bolus, the intravenous infusion of medetomidine

(0.1 mg/kg/hr) was started. All scans were acquired using a 9.4T Biospec MRI system (Bruker BioSpin, Germany) with Paravision 6 software. Throughout the acquisition of the MRI scans, the physiology of the animals was closely monitored. A pressure-sensitive pad (sampling rate 225 Hz; MR-compatible Small Animal Monitoring and Gating system, SA Instruments, Inc., USA) was used to record the breathing rate and the body temperature of the animal was maintained at (37 ± 0.5) °C using a feedback controlled warm air circuitry (MR-compatible Small Animal Heating System, SA Instruments, Inc., USA). Additionally, a pulse oximeter was used to monitor the blood oxygenation (MR-compatible Small Animal Monitoring and Gating System, SA Instruments, Inc., USA). After the acquisition of all MRI scans, an injection of 0.1 mg/kg atipamezole (Antisedan®, Pfizer, Germany) was administered to counteract the effects of the medetomidine anesthesia.

1.3.1 MRI scans acquisition

First, three anatomical multi-slice T2 Turbo-RARE scans (echo time (TE): 11 ms, repetition time (TR): 2500 ms, field of view (FOV): (30 x 30) mm2, matrix [256 x 256], 16 slices of 0.8 mm) were acquired to allow flat skull positioning of the coronal slices. Then, a fourth scan was acquired with the above sequence that served as an anatomical reference scan. Magnetic field inhomogeneity was corrected by local shimming in an ellipsoid volume of interest within the brain. Resting state functional MRI (rsfMRI) scans were acquired with geometrical parameters identical to the anatomical reference scan. The rsfMRI scans started at 35 minutes after the medetomidine bolus injection and were acquired using a T2* weighted echo planar imaging (EPI) sequence (TE: 18 ms, TR: 2000ms, FOV: (30 x 30) mm2, matrix [128 x 96], 16 slices of 0.8 mm). First, a 5-minute baseline rsfMRI was acquired. Second, a 20 minute rsfMRI scan was acquired during which the CNO or vehicle (i.e. saline) was intravenously administered at 5 minutes after the start of the scan. Then, a final 5 minute rsfMRI scan was acquired. These three scans were acquired during one scan session (Fig 2A). Two scan sessions were acquired for each animal in the DREADDs-expressing group, during which the effect of either CNO or vehicle was evaluated. One scan session was acquired for each animal in the control group to evaluate the off-target effects of CNO.

1.3.2 MRI data pre-processing

The pre-processing of the rsfMRI data was performed using Matlab R2014a and SPM12 software (Statistical Parametric Mapping, http://www.fil.ion.ucl.ac.uk). First, all images within each session were realigned to the first image. Second, images were normalized to a study-specific mean EPI template using a global 12 parameter affine transformation followed by the estimation of the non-linear deformations.

Then, a mask excluding the ventricles and all voxels outside the brain was applied to the images. The head motion estimation parameters were regressed out and the images were smoothed in an isotropic manner, with a Gaussian kernel with full width at half maximum of twice the voxel size (0.624 x 0.624 mm). Afterwards, all images were band pass filtered between 0.01 and 0.2 Hz (Zerbi et al., 2015).

1.3.3 MRI data analysis

1.3.3.1 ROI-based analysis

Regions of interest (ROIs) were drawn in brain areas that have been reported to be part of the DMLN in rats, including the cingulate cortex (Cg), orbitofrontal cortex (ORB), prelimbic cortex (PrL), retrosplenial cortex (RS), parietal association cortex (PtPD) and temporal association cortex (TEA) (Lu et al., 2012, Stafford et al., 2014). In addition, ROIs were drawn in regions belonging to the TPN, namely the primary somatosensory cortex (S1), secondary somatosensory cortex (S2), primary motorcortex (M1), secondary motorcortex (M2) and insula (Ins). Separate ROIs for each hemisphere were used in order to be able to discriminate ipsilateral and contralateral effects of right BFB stimulation. The time series of the ROIs, consisting of 4 voxels, were extracted and Pearson correlation coefficients were calculated between each pair of ROIs. Then, these correlation coefficients were Fisher's z-transformed using an in-house program in Matlab. Mean z-transformed matrices were obtained from the DREADDs expressing group after injection of CNO and vehicle as well as from the sham group after injection of CNO. These z-transformed matrices were used to calculate connectivity laterality indices (CLI) for each pair of ROIs as described in (Di et al., 2014).

1.3.3.2 Seed-based analysis

Seed-based analyses were performed in order to assess alterations in whole-brain FC of brain regions that are part of the DMLN. Mean BOLD signal time series were extracted from seed regions using the REST 1.8 toolbox in Matlab. Consequently, the obtained time series was used in a general linear model analysis to compare it to the time series of all other voxels in the brain. Resulting FC maps represent voxels in the brain that significantly correlate to the temporal signal of the seed region. Mean group FC maps were created for each seed region and these maps were also used to make masks including all significant clusters (family-wise correction (FWE) corrected, $p \leq 0.05$, minimal cluster size = 10 voxels). The union of the masks after CNO and vehicle injection in the DREADDs-expressing group was used to extract mean T-values from each animal.

1.3.3.3 Fractional Amplitude of low frequency fluctuations

The fractional amplitude of low frequency fluctuations (fALFF) has previously been used to reflect spontaneous resting state neural activity (Zou et al., 2008). In this study, we obtained fALFF values using the REST 1.8 Toolbox in order to assess resting state neural activity alterations in the DMLN. The time series of each voxel within a seed-based mask (see 4.3.3.2 seed-based mask) was band-pass filtered between 0.01-0.2Hz and these filtered time series were transformed to a frequency domain using a fast Fourier transformation. Then, the obtained power spectrum was used to calculate the fALFF values which can be defined as the ratio of the power within a frequency range (here 0.01 – 0.2Hz) and the total power of the whole frequency range. The mean fALFF values were compared between the CNO and vehicle injection in the DREADDs-expressing group.

1.3.3.4 Statistics

A linear mixed model analysis in JMP Pro13 software was performed to evaluate the effect of administration of CNO or vehicle on FC in the DMLN over time in the DREADDs expressing group and the sham group. In this analysis, the FC in the DMLN of the right hemisphere was compared between the baseline scan and at 5-10 minutes, 10-15 minutes and 15-20 minutes after administration of CNO or vehicle. The subject ID was added in the model as a random variable. Student's T corrections were applied for all multiple comparisons. Further, the FC between ROI pairs in the DMLN and TPN was compared between CNO and vehicle administration in the DREADDs expressing group at 15-20 minutes after injection. A repeated measures Two-way ANOVA with Sidak's multiple comparisons correction was used to evaluate each ROI pair separately. A paired Student's T-test was used to compare the average intra- and inter-hemispheric DMLN FC, the average whole brain FC of seed regions, as well as the fALFF values and CLI after CNO injection or vehicle injection in the DREADDs-expressing animals. An unpaired Student's T-test was used to evaluate intra- and inter-hemispheric DMLN FC alteration between both control groups and between the DREADDs-expressing group and sham group. One-sample Student's T-test were used to make mean seed-based FC maps.

1.4 Immunohistochemistry

1.4.1 Immunofluorescent staining

After the acquisition of all in vivo MRI scans, brain samples 8 rats were collected from rats (N=8) to evaluate the expression of the DREADDs. Rats were deeply anesthetized using an intravenous injection with pentobarbital (Dolethal®, Vetoquinol, Belgium). Then, cardiac perfusion was performed, first with an ice-cold PBS solution and afterwards with a 4% paraformaldehyde solution (Merck Millipore, Merck KGaA, Darmstadt, Germany) for fixation of the tissues. Brains were surgically removed and post-fixed in 4%

paraformaldehyde solution after which a sucrose gradient (5%, 10% and 20% sucrose) was applied. Brains were snap frozen in liquid nitrogen and stored at -80 °C until further processing. Brains were cut into 12 µm sections using a cryostat (Cryostar NX 70, Thermo Fisher Scientific). For the immunofluorescence stainings, the following primary antibodies were used: Sheep Anti-Choline Acetyltransferase (1:500, Abcam; ab18736) and rabbit Anti-m-cherry (1:500, Abcam; ab167453), as well as the following secondary antibodies: Donkey Anti-Sheep (1:200, Abcam; ab150177) and 1:200 Goat Anti-Rabbit (1:200, Abcam; ab7088). Nuclei were counterstained using DAPI (P369350, Thermofischer Scientificx). Stained sections were mounted using Prolonged Gold Antifade.

1.4.2 Image acquisition

The overview images were collected from two animals with a CFI Plan Fluo 10X/0.3 objective on an automated Nikon Ti-E inverted microscope (Nikon Instruments Europe, Amsterdam, The Netherlands) equipped with a SPECTRA light engine® solid-state light source (Lumencor, Beaverton, USA) and a Nikon DS-Qi2 digital camera. Nikon NIS-elements software was used to control the image acquisition and stitching. The representative confocal images of 3 animals were taken with a Leica TCS SP8 confocal laser scanning microscope (Leica-microsystems, Wetzlar, Germany). Blue fluorescence was obtained with 405 nm diode laser and PMT detector. A white light laser (excitation wavelength of 488 nm for green fluorescence (Alexa Fluor®488) and 596 nm for red fluorescence (Texas Red®)) and a HyD dectector were used to visualize green and red fluorophores. Z-stacks were acquired with a 0.5 µm interval (HC PL APO CS2 63X/1.20 water). Images were acquired with a resolution of [1024 x 1024] pixels.

2. Supplementary figures

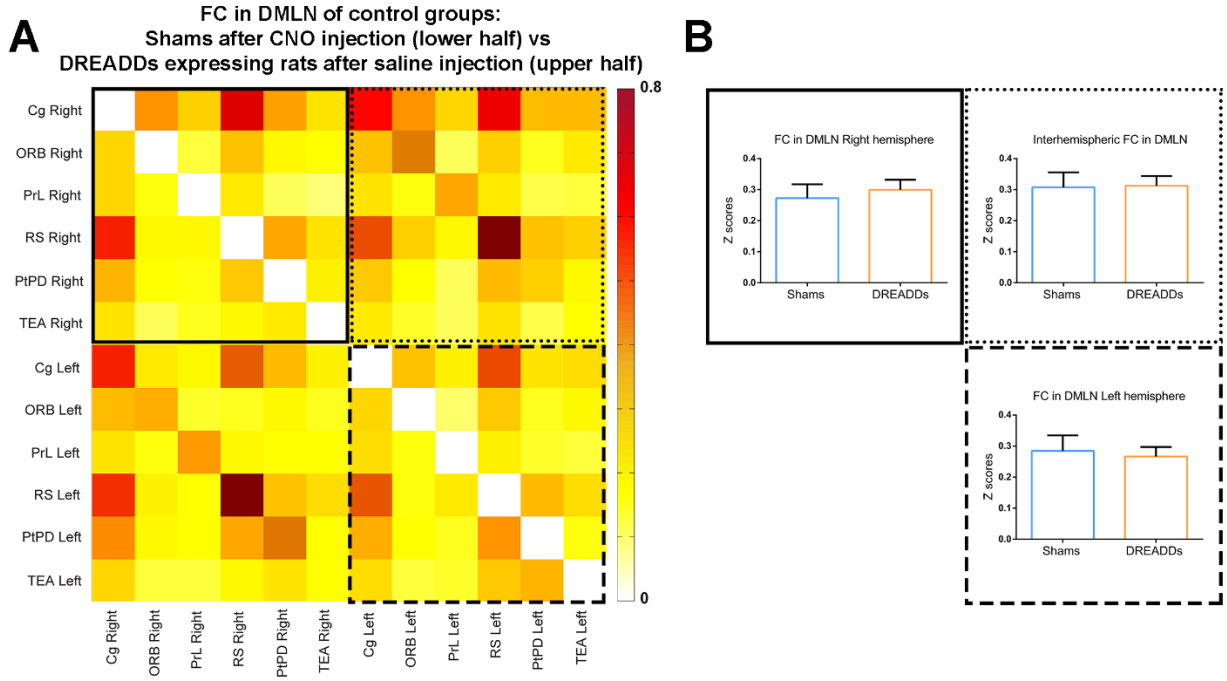

Supplementary figure 1. DMLN ROI-based analysis in the control groups: sham group after CNO injection and DREADDs expressing rats after saline injection, related to figure 2 *(A) Pairwise z-transformed FC matrix after CNO injection in the sham group (sub-diagonal) and after saline injection in the DREADDs-expressing rats (supra-diagonal). The colour bar represents z-scores. No significant differences between the two control groups were found (Two-way ANOVA with Sidak's correction for multiple comparisons). (B) Bar-graphs of the average intra-hemispheric FC (z-scores) in the DMLN of the right hemisphere and left hemisphere, as well as the average inter-hemispheric FC of the DMLN. The z-scores of the two groups were statistically compared using an unpaired Student's T-test. Data are represented as mean +/- SEM. Abbreviations: cingulate cortex (Cg), orbitofrontal cortex (ORB), prelimbic cortex (PrL), retrosplenial cortex (RS), parietal association cortex (PtPD), temporal association cortex (TEA), functional connectivity (FC), default mode-like network (DMLN), clozapine-N-oxide (CNO), designer receptors exclusively activated by designer drugs (DREADDs).*

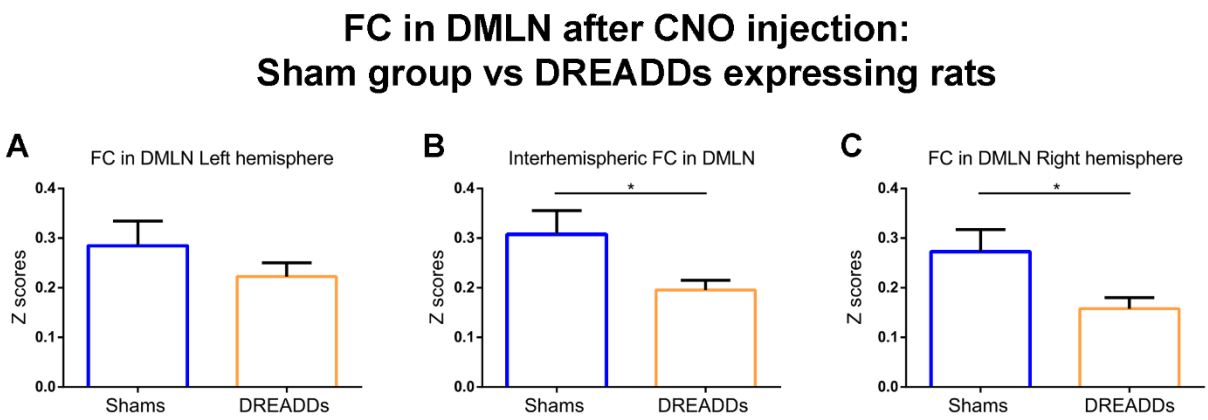

Supplementary figure 2. ROI-based analysis assessing average FC in the DMLN after CNO injection in the sham group and the DREADDs-expressing rats, related to figure 3 *Panels represent the average intra-hemispheric FC (z-scores) of the DMLN in the left hemisphere (A) and right hemisphere (C), as well as the inter-hemispheric FC (z-scores) of the DMLN (B). The average FC values were statistically compared between both groups using an unpaired Student's T-test. Data are represented as mean +/- SEM.* p≤0.05. Abbreviations: functional connectivity (FC), default mode-like network (DMLN), clozapine-N-oxide (CNO), designer receptors exclusively activated by designer drugs (DREADDs).*